



The geometrical parameters include the wheelbase  $l$  and the distance  $b$  between points R and G. The vehicle mass is denoted by  $m$ , while  $J_G$  is the yaw moment of inertia about the center of mass and  $J_F$  denotes the mass moment of inertia of the steering system.

Deriving the equations of motion of the vehicle model using the Appell-Gibbs method (see [13] for details) leads to

$$\dot{x}_R = V \frac{\cos \psi}{\cos \gamma} - \sigma \frac{\sin(\psi+\gamma)}{\cos \gamma} - l\omega \cos \psi \tan \gamma, \quad (1)$$

$$\dot{y}_R = V \frac{\cos \psi}{\cos \gamma} + \sigma \frac{\cos(\psi+\gamma)}{\cos \gamma} - l\omega \sin \psi \tan \gamma, \quad (2)$$

$$\dot{\psi} = \omega, \quad (3)$$

$$\dot{\gamma} = \Omega, \quad (4)$$

and

$$\begin{bmatrix} m_{11} & m_{12} & 0 \\ m_{21} & m_{22} & J_F \\ 0 & J_F & J_F \end{bmatrix} \begin{bmatrix} \dot{\sigma} \\ \dot{\omega} \\ \dot{\Omega} \end{bmatrix} = \begin{bmatrix} f_1 \\ f_2 \\ f_3 \end{bmatrix}, \quad (5)$$

where  $\sigma$  is the lateral velocity of point R,  $\omega$  is the yaw rate of the vehicle, and  $\Omega$  is the steering rate. The generalized mass matrix includes the elements

$$m_{11} = \frac{m}{\cos^2 \gamma}, \quad (6)$$

$$m_{12} = m_{21} = m(b + l \tan^2 \gamma), \quad (7)$$

$$m_{22} = J_G + J_F + m(b^2 + l^2 \tan^2 \gamma). \quad (8)$$

The right-hand side of Eq. (5) consists of

$$f_1 = \frac{F_F}{\cos \gamma} + F_R - \frac{m}{\cos \gamma} (V - (l - b)\omega \sin \gamma)\omega + \frac{m \sin \gamma}{\cos^3 \gamma} (V \sin \gamma - \sigma - l\omega)\Omega, \quad (9)$$

$$f_2 = \frac{F_{Fl}}{\cos \gamma} - \frac{m}{\cos \gamma} (bV + (l - b)\sigma \sin \gamma)\omega + \frac{ml \sin \gamma}{\cos^3 \gamma} (V \sin \gamma - \sigma - l\omega)\Omega + M_F + M_R, \quad (10)$$

$$f_3 = M_F + M_S. \quad (11)$$

The lateral tire forces  $F_F$  and  $F_R$ , as well as the self-aligning moments  $M_F$  and  $M_R$  are considered as functions of the side-slip angles

$$\tan \alpha_F = -\frac{\sigma + l\omega}{V \cos \gamma} + \tan \gamma, \quad (12)$$

$$\tan \alpha_R = \frac{V \cos \gamma}{-V + (\sigma + l\omega) \sin \gamma} \quad (13)$$

using the nonlinear brush tire model, as detailed in [13].

In order to ensure stable path following, a higher-level controller is designed in this paper to follow the straight-line reference path along the  $x$  axis. Thus, the desired steering angle  $\gamma_{des}$  is calculated using the feedback of the lateral position  $y_R$  and the course angle  $\theta$  of the rear axle center point:

$$\gamma_{des} = -k_y y_R(t - \tau) - k_\theta \sin(\theta(t - \tau)), \quad (14)$$

where  $\tau$  is the feedback delay, which includes sensor and communication delays, data processing time and

actuation delay. The course angle is calculated as  $\theta = \psi - \alpha_R$ , and  $k_y$  and  $k_\theta$  are the control gains. The tracking performance of this simple controller can be improved in case of varying path curvature by adding a feedforward term, as in e.g. [14].

In order to realize the desired steering angle, the steering torque  $M_S$  is generated according to the lower-level PID controller

$$M_S = -k_p(\gamma - \gamma_{des}) - k_d \dot{\gamma} - k_i z, \quad (15)$$

where  $k_p$ ,  $k_d$  and  $k_i$  are the lower-level control gains and

$$z = \gamma - \gamma_{des}. \quad (16)$$

It has been shown in [15] that as long as the time delay in the lower-level controller is below a critical value of  $\sim 1$  ms, it has negligible effects on the stability of the system, therefore it will not be considered in our analysis.

### 3. NONLINEAR ANALYSIS

The resulting system of delay differential equations (1-16) of the controlled vehicle is analyzed with the help of the DDE-Biftool software package [16,17]. Subcritical Hopf bifurcations are detected along the stability boundaries in the plane of the control gains  $k_y$  and  $k_\theta$ . The periodic orbits emerging from these bifurcation points are followed using numerical continuation within the entire linearly stable parameter domain of the control gains.

The bifurcation diagrams in Fig. 2 (a) and (b) show the limit cycle amplitudes in terms of the lateral position  $y_R$  as a function of the control gain  $k_\theta$  for the vehicle parameters listed in Table 1. It can be seen that the linearly stable range of  $k_\theta$  is bounded by Hopf bifurcation points on both sides which are connected by an unstable periodic orbit. As shown in the bifurcation diagrams, for larger control gains, the amplitude of the unstable limit cycle is smaller, suggesting a smaller basin of attraction for stable path following. This means that if the vehicle is sufficiently perturbed, the controller will not be able to steer the vehicle back towards the reference path, even if the closed-loop system is stable in the linear sense.

The color coding in Fig. 2 (c) shows how the unstable limit cycle amplitudes change inside the linearly stable parameter domain of both control gains, up to 2 meters in terms of the lateral position  $y_R$ . Points where the limit cycle amplitudes are above 2 meters are considered safe, since in these cases the controller can handle larger perturbations too. The corresponding safe zone of control gains is shaded in gray in Fig. 2 (c).

Observe that a large part of the linearly stable parameter domain falls outside of this safe zone. This means that the system can leave the basin of attraction of the stable solution in these cases for sufficiently large perturbations, which is a severe safety issue in practice.

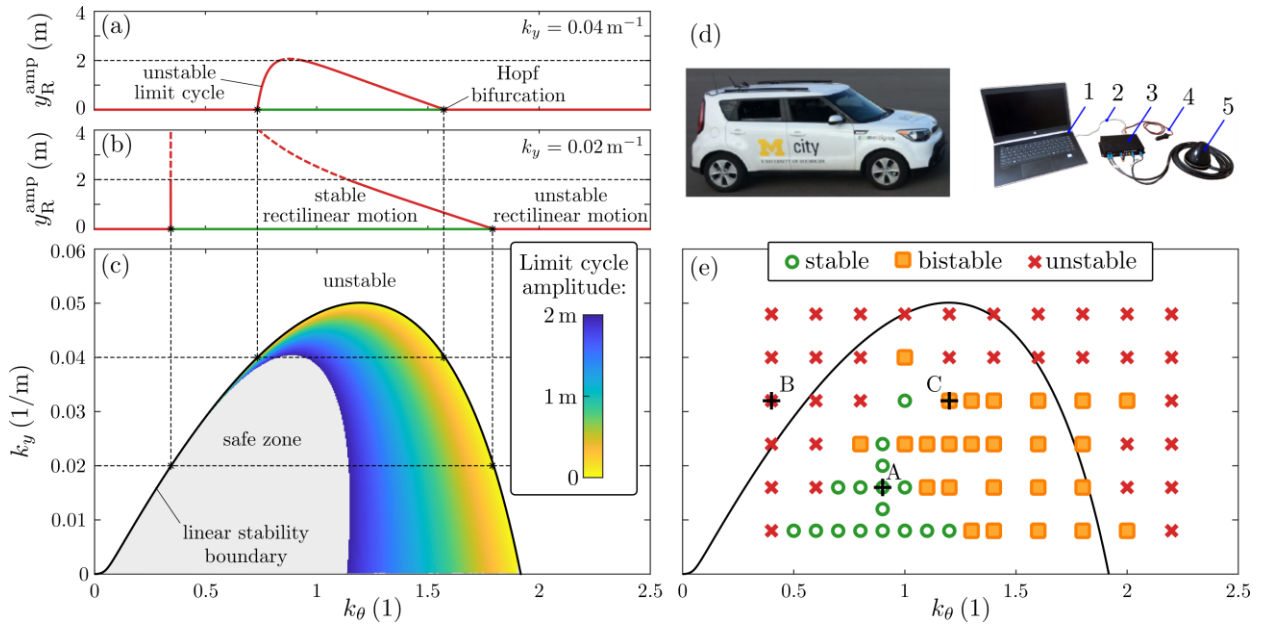


Fig. 2 (a)-(b) Bifurcation diagrams of the controlled vehicle. (c) Unstable limit cycles around the linearly stable domain of control gains. The coloring refers to the unstable limit cycle amplitudes. (d) The vehicle and the V2X measurement setup used in the experiments - 1: host computer, 2: network cable, 3: electronic control unit, 4: power cable, 5: antennae. (e) Experimental results.

Table 1 Vehicle Parameters

wheelbase	$l$	2.57 m
distance between rear axle and center of gravity	$b$	1.54 m
vehicle mass	$m$	1770 kg
yaw moment of inertia	$J_G$	1343 kgm <sup>2</sup>
steering system moment of inertia	$J_F$	0.25 kgm <sup>2</sup>
lower-level steering control proportional gain	$k_p$	640 Nm
lower-level derivative gain	$k_d$	8 Nms
lower-level integral gain	$k_i$	40 Nm/s
tire contact patch half-length	$a$	0.1 m
tire cornering stiffness	$C$	40 kN
sliding friction coefficient	$\mu$	0.6 -
rolling friction coefficient	$\mu_0$	0.9 -
longitudinal velocity	$V$	15 m/s
feedback delay	$\tau$	0.7 s

#### 4. EXPERIMENTAL VALIDATION

In order to validate the results of the theoretical analysis, a series of real vehicle experiments were performed at the Mcity test track of the University of Michigan. The test vehicle (shown in panel (d) of Fig. 2) was equipped with a GPS device mounted at the rear axle center point. The experiments were aimed at demonstrating the feasibility of motion control relying on vehicle-to-everything (V2X) communication only, in cases when the onboard sensors fail [13]. This means that the applied control algorithms must be able to handle less frequent data transfer and less accurate sensor data. In

case of the GPS device used in the experiments, the satellite data was upgraded only every 1 sec (with state estimations in-between) with an accuracy of approximately 0.7 m.

The experiments were performed for different combinations of the higher-level control gains, where the vehicle aimed to follow the lane centerline of a straight multi-lane segment of the test track, relying on GPS data. For each control gain combination in Fig. 2 (e), three different measurements were carried out. Depending on the behavior of the vehicle, the individual measurement points were labelled as either stable (green circles in Fig. 2 (e)), bistable (orange squares) or unstable (red crosses). For the gain combinations labelled as stable, the lane-keeping controller was working as intended in all three test runs, with decaying oscillations. In the measurement points labelled as bistable, solutions with increasing and decreasing lateral oscillations were both observed presumably due to the non-uniform initial conditions and measurement noise. Finally, in the points labelled as unstable, the vehicle was not able to successfully follow the lane centerline in any of the test runs.

Figure 3 shows some representative time series data of the lateral position of the vehicle in the measurement points marked in Fig. 2 (e). Figure 3 (a) shows a stable measurement (using the gains at point A), where the vehicle tended towards the reference path even from a relatively large initial condition. In panel (b), the control gains were selected from the theoretically unstable region (point B), which resulted in an oscillatory stability loss even when the vehicle was started close to the reference path. Panel (c) shows an example of the bistable behavior observed during the measurements (point C): for a small initial perturbation, the vehicle safely follows the reference path, but a slightly larger initial error leads to stability loss.

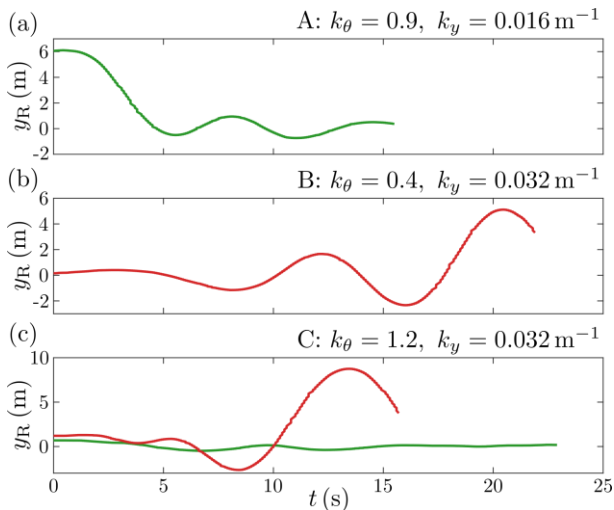


Fig. 3 Measured time series of the vehicle lateral position  $y_R$  for the experiments corresponding to points A, B and C in Fig. 2 (e).

### 5. CONCLUSION

The bifurcation analysis of the lane-keeping control of automated vehicles was performed in this paper. Using numerical continuation, unstable limit cycles have been identified along the linearly stable domain of control gains. The oscillation amplitude of these periodic orbits around the equilibrium of stable path following can be used as an indicator of the robustness of the controller against perturbations. Based on the results of the nonlinear analysis, a safe zone of control gains has been identified, where the controlled vehicle is able to safely handle larger perturbations.

The results have been verified using a series of real vehicle experiments on a test track. The measurement results confirm the importance of taking into account the time delay as well as the nonlinear effects in the control design. Consistently stable measurements were only achieved in the region of the stable domain where the amplitude of the unstable limit cycle was sufficiently large. Stable operation can still be achieved outside of this region, but the system was demonstrated to be more susceptible to perturbations and noise, which may lead to serious safety hazards in practice.

### REFERENCES

[1] Olofsson, B. et al., "Using crash databases to predict effectiveness of new autonomous vehicle maneuvers for lane-departure injury reduction", *IEEE Trans. on ITS*, 2020, doi: 10.1109/TITS.2020.2983553.

[2] Heredia, G. et al., "Stability of autonomous vehicle path tracking with pure delays in the control loop", *AR*, 2007, doi: 10.1163/156855307779293715.

[3] Vörös, I. et al., "Lane-keeping control of automated vehicles with feedback delay: Nonlinear analysis and laboratory experiments", *EJoM - A/Solids*, 2022, doi: 10.1016/j.euromechsol.2022.104509.

[4] Della Rossa, F. et al., "Bifurcation analysis of an automobile model negotiating a curve", *VSD*, 2012, doi: 10.1080/00423114.2012.679621.

[5] Shen, S. et al., "Nonlinear dynamics and stability analysis of vehicle plane motions", *VSD*, 2007, doi: 10.1080/00423110600828285.

[6] Steindl, A. et al., "Limit cycles at oversteer vehicle", *ND*, 2020, doi: 10.1007/s11071-019-05081-8.

[7] Della Rossa, F. et al., "Analysis of the lateral dynamics of a vehicle and driver model running straight ahead", *ND*, 2018, doi: 10.1007/s11071-017-3478-1.

[8] Mastinu, G. et al., "Straight running stability of automobiles: experiments with a driving simulator", *ND*, 2020, doi: 10.1007/s11071-019-05438-z.

[9] Liu, Z. et al., "Stability and oscillations in a time-delayed vehicle system with driver control", *ND*, 2004, doi: 10.1023/B:NODY.0000021080.06727.f8.

[10] Li, S. E. et al., "Predictive lateral control to stabilise highly automated vehicles at tire-road friction limits", *VSD*, 2020, doi: 10.1080/00423114.2020.1717553.

[11] Wurts, J. et al., "Collision imminent steering at high speed using nonlinear model predictive control", *IEEE Trans. on CST*, 2020, doi: 10.1109/TVT.2020.2999612.

[12] Berntorp, K. et al., "Trajectory tracking for autonomous vehicles on varying road surfaces by friction-adaptive nonlinear model predictive control", *VSD*, 2020, doi: 10.1080/00423114.2019.1697456.

[13] Beregi, S. et al., "Connectivity-based delay-tolerant control of automated vehicles: theory and experiments", *IEEE Trans. on IV*, 2021, doi: 10.1109/TIV.2021.3131957.

[14] Qin, W. B. et al., "Dynamics and control of automobiles using nonholonomic vehicle models", *arXiv preprint*, 2021, doi: 10.48550/arXiv.2108.02230.

[15] Beregi, S. et al., "Hierarchical steering control for a front wheel drive automated car", *IFAC-PapersOnLine*, 2018, doi: 10.1016/j.ifacol.2018.07.189.

[16] Engelborghs, K. et al., "Numerical bifurcation analysis of delay differential equations using DDE-BIFTOOL", *Trans. on MS*, 2002, doi: 10.1145/513001.513002.

[17] Engelborghs, K. et al., "DDE-BIFTOOL v. 2.00: a Matlab package for bifurcation analysis of delay differential equations", *TW Reports*, 2001, 61-61.

### ACKNOWLEDGEMENTS

The research reported in this paper was partly supported by the János Bolyai Research Scholarship of the Hungarian Academy of Sciences and by the National Research, Development and Innovation Office of Hungary under grant no. NKFI-128422 and under grant no. 2020-1.2.4-TÉT-IPARI-2021-00012. The authors also acknowledge the support provided by Mcity at the University of Michigan.